# Electronic Supplementary Information

## Nonlocal electron-phonon coupling in prototypical molecular semiconductors from first principles

Xiaoyu Xie,[†,‡] Alejandro Santana-Bonilla,[†] and Alessandro Troisi[†]

†*Department of Chemistry, University of Liverpool, Liverpool L69 3BX, UK*

‡*School of Chemistry and Chemical Engineering, Nanjing University, Nanjing 210023, China*

E-mail:

# 1 Validation of the DFTB methodology

In order to validate the calculations obtained throughout this work using the DFTB+ code,[1] we have carried out a series of calculations of molecular and crystalline properties employing Gaussian and Quantum-Espresso DFT-implementations.[2] Thus, we started by relaxing the structures both in gas- and crystal- phases. In the gas-phase case, the results are assessed by comparing the DFTB+ outputs with the all-electron implementation.[2] For this case, we focused our study in the distribution of the energy levels and their corresponding molecular orbitals. Also, the vibrational modes for both molecules have been computed establishing the accuracy of DFTB+[1] to describe molecular mechanical properties. In the case of crystalline phases, we assessed the accuracy by computing the phonon band structure for tetracene crystalline structure and compared with the plane-wave software Quantum-Espresso.

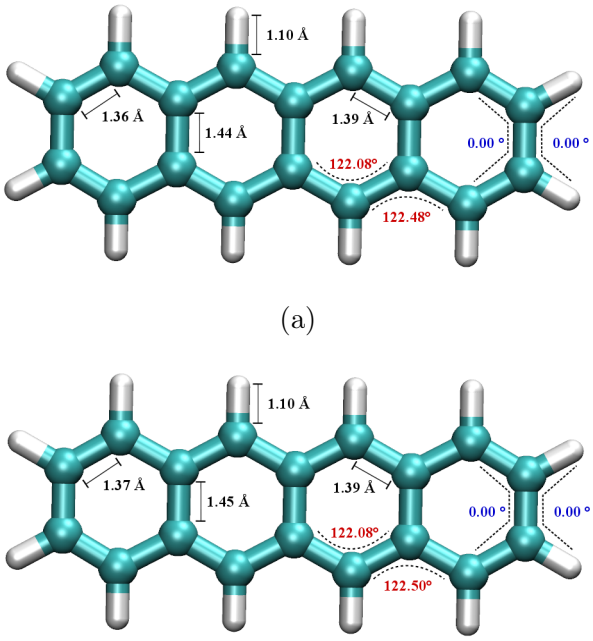


(a)

(b)

Figure 1: Relaxed gas-phase structures (tetracene) for (a) G09 and (c) DFTB+. Selected bonds (black) and angles (red for bonds and blue for dihedral) are highlighted.

## 1.1 Gas-Phase Electronic structure and vibrational frequencies of Tetracene

The relaxed structures computed by (a) DFTB+, (b) G09 and methodologies are displayed in Figure 1. As a result of this procedure, one can observe that the bond values computed by DFTB+ are close to those obtained from the all-electron DFT calculations employing the B3LYP/6−311G* level of theory (Figure 1(a,b)). Similarly, we report that the energy differences computed for selected energy levels,namely, HOMO, HOMO-1 and HOMO-2 and the corresponding wavefunctions are in good agreement as is shown in Table 1.

Finally, we carried out excited state calculations in order to estimate the capability and accuracy of DFTB+ to describe accurately HOMO-LUMO gap. As presented in Figure 2 there is a reasonable agreement between the Casida implementation used in DFTB+ [1] and the TDDFT calculations carried out in G09. [2] The excitation symmetry coincides in both implementations. The underestimation of the HOMO-LUMO gap can be ascribed to the

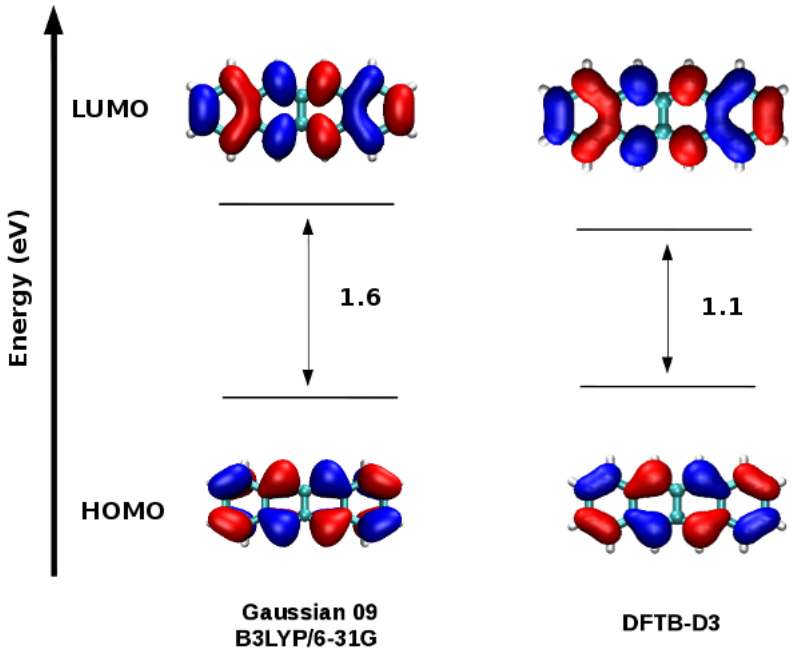


Figure 2: Gas-Phase molecular diagram for HOMO and LUMO electronic energy levels including the associated wavefunctions for each energy level.

lack of a bigger basis-set experienced in the DFTB methodology which can be improved by creating better slater-koster files with the aim to describe accurately such properties.

Thus, in terms of the geometries and the electronic structure description of the gas-phase tetracene molecule, we obtain a reasonable agreement between the two methodologies highlighting the good agreement between the DFTB approach once is compared with the all-electron reference calculation (for the actual values see Table 2). In the case of the LJ implementation, we notice a constant underestimation of the value of the frequencies which can ascribed to the origin of such approximation whose contributions are independently computed after a SCC–DFTB cycle has been carried out and added to the total energy.

## 1.2 Gas-Phase Electronic structure and vibrational frequencies of Rubrene

In terms of bond distances and bond angles (Figure 3), we observe a good agreement between the discussed methodologies. In the case of dihedral angles, there is a small discrepancy

Table 1: energy differences (in eV) for tetracene complex. The HOMO-LUMO gap has been calculated using TDDFT which in the case of DFTB is computed using the Casida formulation. In both cases we can observe the good agreement between the different methodologies in which the HOMO molecular orbital displays a bonding character while the LUMO level shows an antibonding shape.

| Method | $\Delta E_{Homo-Homo-1}$ | $\Delta E_{Homo-1-Homo-2}$ | $\Delta E_{Homo-Lumo}$ |
|---|---|---|---|
| DFTB+ | 1.14 | 0.107 | 1.6 (Triplet) |
| B3LYP/6-311G | 1.46 | 0.09 | 1.1 (Triplet) |

Table 2: Vibrational frequencies ($cm^{-1}$) of the tetracene molecule in gas-phase. The computed values are compared between the different levels of theory, ranging from DFTB+ where the dispersion forces are included by a Lennard-Jones potential (LJ), to the semi-empirical implementation using the Grimmes-D3 as is included in DFTB+. Also, all-electron (AE) computed frequencies are reported.

| Mode | DFTB-(LJ) | DFTB-(D3) | DFT(B3LYP) |
|---|---|---|---|
| 1 | 39 | 51 | 55 |
| 2 | 74 | 86 | 89 |
| 3 | 128 | 139 | 149 |
| 4 | 167 | 168 | 163 |
| 5 | 174 | 184 | 191 |
| 6 | 237 | 254 | 270 |
| 7 | 297 | 306 | 304 |
| 8 | 311 | 309 | 317 |
| 9 | 329 | 325 | 317 |

between the results calculated by G09 and DFTB where small torsion of the tetracene core is observed in the all-electron calculation while total planarity is reported by the DFTB approach. In the case of the electronic structure computations, reasonable agreement is found in terms of the energy difference for selected molecular levels which are reported in Table 3.

Finally, we carried out excited state calculations for Rubrene in gas-phase and the results are presented in Figure 4. There is a reasonable agreement between the DFTB+ and the TDDFT calculations carried out in G09.[2] The symmetry of the excitation (triplet) is correctly described in DFTB+. The underestimation of the HOMO-LUMO gap can be ascribed to the lack of a bigger basis-set which can describe Rydberg states important in these

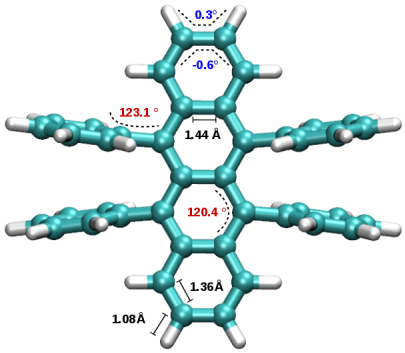


(a)

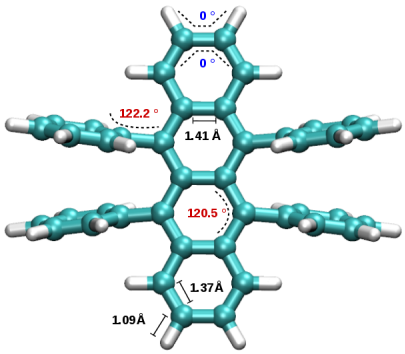


(b)

Figure 3: Relaxed gas-phase structures (Rubrene) for (a) G09 and (b) DFTB+. Selected Bonds (black) and Angles (red for bonds and blue for dihedral) are highlighted.

kind of big molecules. However, the DFTB methodology can be improved by creating better slater-koster files with the aim to describe accurately excited-state molecular properties.

To conclude, in terms of the geometries and the electronic structure description of the gas-phase rubrene molecule, we obtain a reasonable agreement between the two methodologies. In the case of the gas-phase vibrational frequencies, when compared with the all-electron DFT results, one can observe that the DFTB-D3 and the Lennard-Jones implementation are in reasonable agreement with reference values (B3LYP/6-31G) (for the actual values see Table 4). The main discrepancies can be ascribed to differences in the molecular forces computed with DFTB+ which lack of additional states present in the all-electron implementation that can provide a better description of the Rydberg-states.

Table 3: Molecular energy differences (in eV) for rubrene complex. The HOMO-LUMO gap has been calculated using the TDDFT methodology which in the case of DFTB is implemented using the Casida formulation.

| Method | $\Delta E_{Homo-Homo-1}$ | $\Delta E_{Homo-1-Homo-2}$ | $\Delta E_{Homo-Lumo}$ |
|---|---|---|---|
| DFTB+ | 1.02 | 0.13 | 1.49 (Triplet) |
| B3LYP/6-311G | 1.3 | 0.05 | 1.05 (Triplet) |

Table 4: Vibrational frequencies ($cm^{-1}$) of the rubrene molecule in gas-phase. The computed values are compared between the different levels of theory, ranging from DFTB+ where the dispersion forces are included by either the Lennard-Jones potential (LJ) or the semi-empirical implementation using the Grimme-D3. Also here, planewave (PW) and all-electron (AE) computed frequencies are reported as reference points to assess the accuracy of the methodology.

| Mode | DFTB-(LJ) | DFTB-(D3) | DFT(B3LYP)(AE) |
|---|---|---|---|
| 1 | 15 | 9 | 6 |
| 2 | 18 | 19 | 22 |
| 3 | 21 | 23 | 24 |
| 4 | 48 | 37 | 62 |
| 5 | 50 | 42 | 65 |
| 6 | 57 | 57 | 67 |
| 7 | 60 | 60 | 70 |
| 8 | 76 | 72 | 74 |
| 9 | 82 | 79 | 77 |

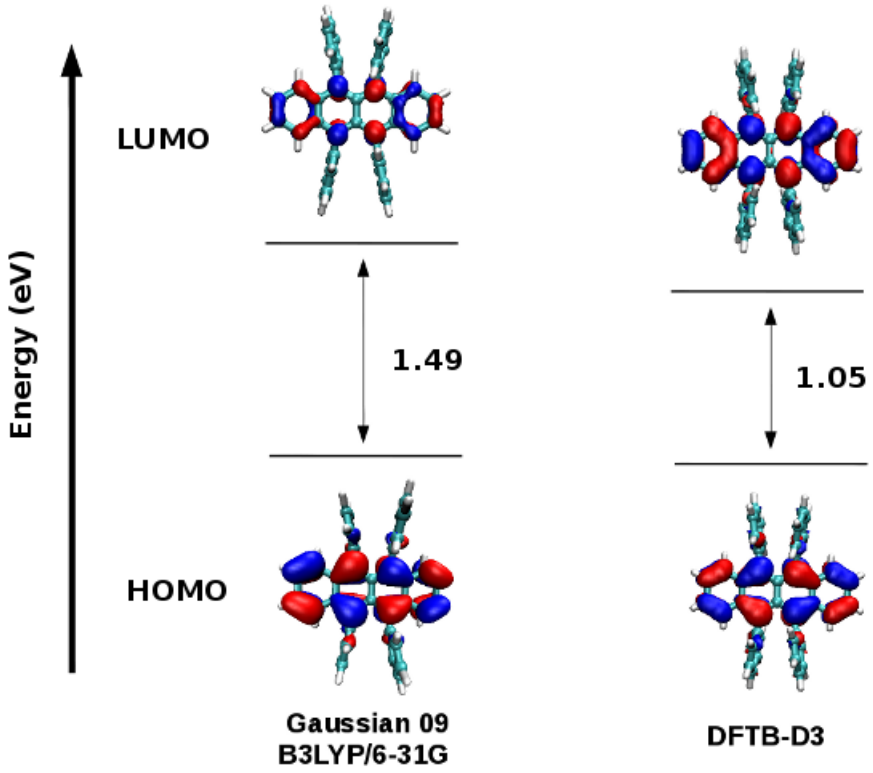


Figure 4: Gas-Phase molecular diagram for HOMO and LUMO electronic energy levels including the associated wavefunctions for each Energy level.

# 2 Mechanical properties of crystalline phases

In this section, we perform calculations of the mechanical properties of the tetracene and rubrene molecular crystals comparing the phonon band structure in the case of tetracene obtained with DFTB+ and compared with both established methodologies and computations reported in literature.[3] This is a crucial issue since the correct description of the mechanical properties (phonon dispersion relations)depends on a complex interplay between molecular packing, provided by the underlying lattice, and the weak vdW forces which holds the molecules together.

## 2.1 Phonon band structures for tetracene

In order to establish the accuracy of our methodology to describe the phonon behavior at different points in the q-space the phonon band structure has been computed as is explained in the main text. These results have been compared with calculations carried out by employing the plane-wave code Quantum-Espresso where the exchange-correlation C09-vdW-DF2 implementation has been used.[4,5] A cut-off energy of 30 Ry in an electronic mesh of $8 \times 8 \times 8$ employing the Monkhorst-Pack scheme has been used to relax both the lattice and atomic positions of the system. The structure is considered relax when the Helmann-Feynman forces are below $1 \times 10^{-6}$ Ry/bohr and the total energy to $1 \times 10^{-12}$ Ry has been reached. The self-consistent calculations threshold for all self-consistent calculations is set to $1 \times 10^{-12}$ Ry. The tetracene phonon band structure calculation has been performed on the relaxed structure unit cell by employing the DFPT.[6] The self-consistent calculation threshold is set to $1 \times 10^{-12}$ Ry. Fourier interpolation technique of the obtained Dynamical matrices has been used to construct the continuous sampling of the q-space. The high-symmetry points used are $\Gamma = (0, 0, 0)$, B $= (0.5, 0, 0)$, F $= (0, 0.5, 0)$, G $= (0, 0, 0.5)$, Z $= (0, 0.5, 0.5)$ and K $= (0.5, 0.5, 0)$ which scans the full extension of the irreducible Brillouin zone. The results of both calculations are presented in Figure 5. Our comparison is focused on the description

of low-frequency normal modes which are below 200 $cm^{-1}$ which are the associated modes active at room temperature. In general terms both phonon band structures are describing the same phonon behaviour along the selected high-symmetry points. However, some discrepancies in the description of the three lowest normal modes (acoustic) are observed specially at the $B-K$, $G-Z$ and $Z-F$ connection paths that can be ascribed to small variations of the forces computed from the variation in the electronic density due to the minimal basis set used in the DFTB approach. In frequency regions above 50 $cm^{-1}$ the curvature of the phonon band strictures is similar leading us to conclude the suitability of DFTB vdw-D3 approach to describe mechanical properties of organic semiconductors.

## 2.2 Phonon band structures for rubrene

In the main text we restrict ourselves to the presentation of the phonon band structure between the $\Gamma$ and the S high-symmetry points of the Brillouin zone. However, the irreducible Brillouin zone commonly used to display the electron band structure contains more high-symmetry points. Therefore, in Figure 6 we present the complete phonon band structure along the the high-symmetry path $\Gamma = (0, 0, 0)$, $S = (0, 0.5, 0)$, $T(0, 0.5, 0.5)$, $Z = (0, 0, 0.5)$ and $Y = (0.5, 0, 0)$. The frequency range chosen to depict the band structure corresponds to energies around room temperature $\simeq k_B T$. It is interesting to notice how intricate interactions between different branches in the path $\Gamma - S$ is rather simplified when compared with the path $S - T$ where many modes become degenerated. The degeneracy is lifted when the q-space path is take from $T - Z$ where several branches are observed until the end of the Brillouin zone. Finally, the path $\Gamma - Y$ depicts the same behaviour of a manifold of branches as the the first segment of the irreducible Brillouin zone along a direction in which no transfer integrals are important but being a possible channel in which heat can be either transported or dissipated.

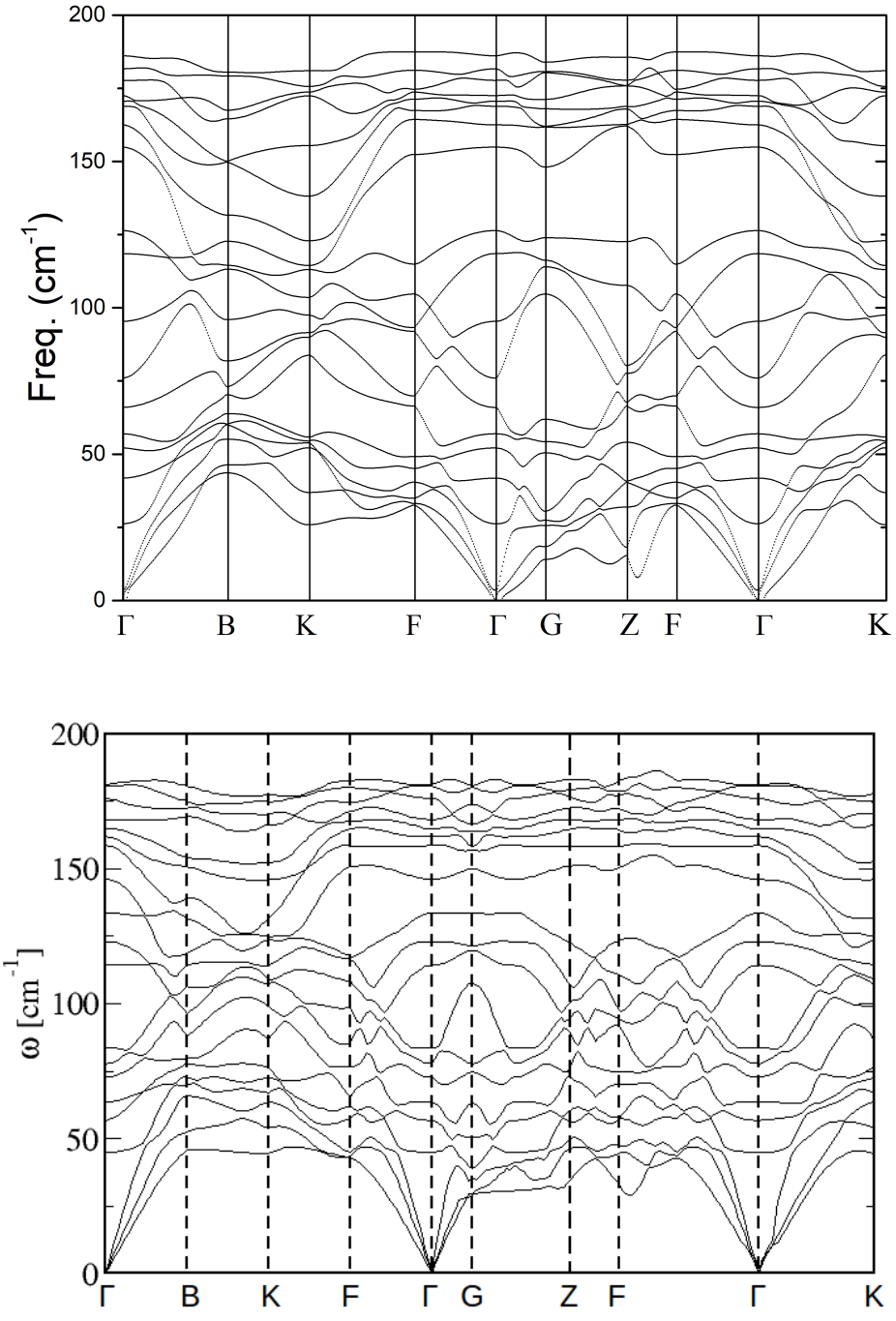


Figure 5: Computed phonon band structures for tetracene molecular crystal employing (a) DFTB vdW-D3 and (b) c09-vdW-DF2 implementations. All high-symmetry points have been selected to represent accurately the full Brillouin-zone in the reciprocal space.

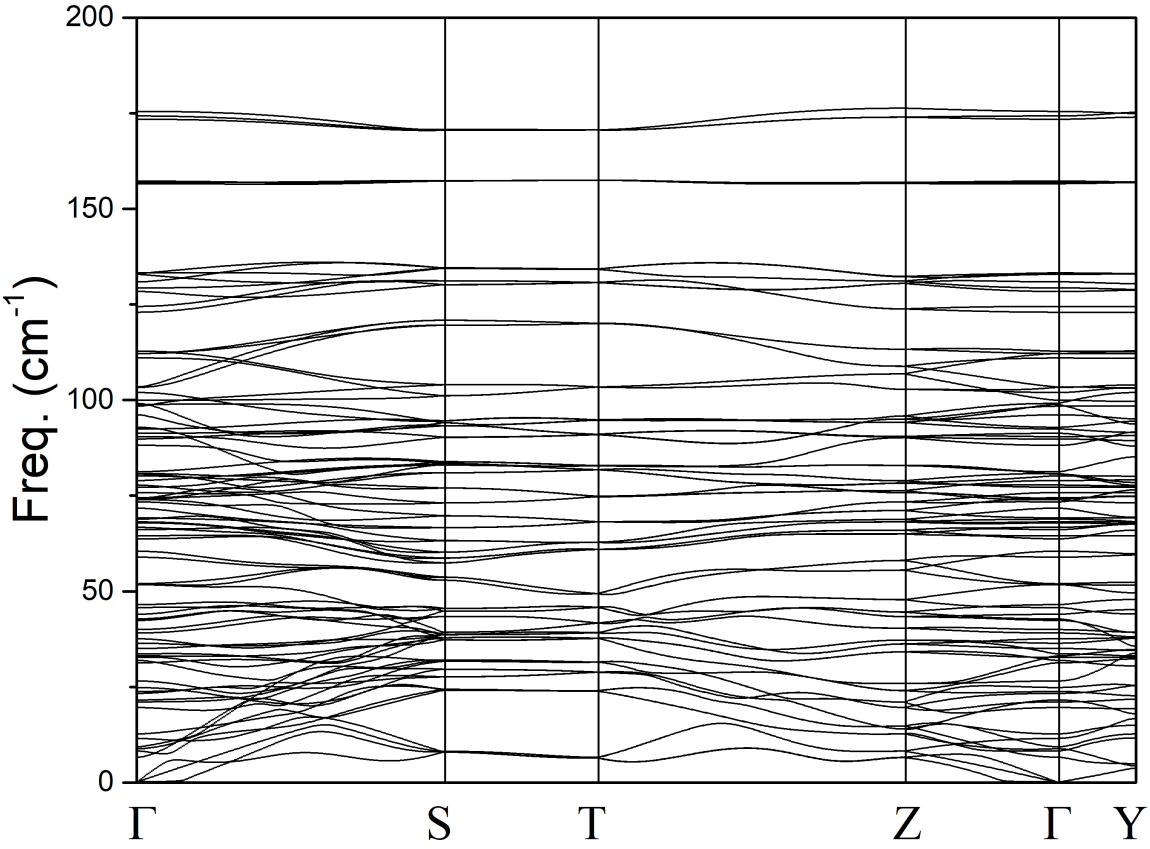


Figure 6: Computed phonon band structures for rubrene molecular crystal employing DFTB vdW-D3 implementations. All high-symmetry points have been selected to represent accurately the full Brillouin-zone in the reciprocal space.

# 3 Nonlocal electron-phonon coupling

Formally, the electron-phonon coupling describes the change in the electronic structure of a system ascribed to a change of its geometry. Therefore, the electron Hamiltonian elements (e.g. transfer integral in our case) can be computed from a microscopically viewpoint by performing a simple Taylor series expansion as a function of the normal modes of the system in terms of the normal coordinates as:

$$t = t_0 + \sum_I g^I Q_I + \sum_{I,J} \chi^{I,J} Q_I Q_J + \dots \tag{1}$$

where,

$$g^I = \frac{\partial t}{\partial Q_I}, \tag{2}$$

$$\chi^{I,J} = \frac{\partial^2 t}{\partial Q_I Q_J} \tag{3}$$

The displacements along the corresponding normal modes are represented by $Q_I$. In this case, we applied a linear approximation for Equation (1) which leads to the following expression,

$$t = t_0 + \sum_I g^I Q_I \tag{4}$$

Considering the supercell approach used in this work for the calculation of phonon normal modes, the number of phonon modes depend on the sampling number of $\mathbf{q}$ points. In our case, an assumption that the transfer integrals are effected by the dimer systems only is used. Therefore, we expand transfer integral using a complete basis set of displacement $\{\mathbf{B}_i\}$ for the dimer system and calculate the first derivatives of the electronic coupling with respect to this basis set first,

$$t = t_0 + \sum_i g^{i,0} B_i \quad \text{with} \quad g^{i,0} = \frac{\partial t}{\partial B_i} \tag{5}$$

where $g^{i,0}$ represents the first derivative and $i = 1, 2, \dots, 3N_{atom}$ ($N_{atom}$ is the number of

atoms in the dimer system). Additionally, the total system can be subdivided in terms of the molecules which are relevant for the electron transfer process and whose associated normal modes $\{\mathbf{Q}_I\}$ $(I = 1, 2, \ldots, N_{mode})$ can be rotated to the vector space of $\{\mathbf{B}_i\}$ and redundancy part which would not effect the transfer integral,

$$\mathbf{Q}_I = \sum_i R_{Ii}\mathbf{B}_i + \text{rest} \tag{6}$$

It is obvious that,

$$g^I = \frac{\partial t}{\partial Q_I} = \sum_i \frac{\partial t}{\partial B_i}\frac{\partial B_i}{\partial Q_i} = \sum_i g^{i,0} R_{Ii} \tag{7}$$

For convenience, we have selected the atomic coordinates as the basis set, i.e.

$$\{B_i\} = \{x_1, y_1, z_1, \ldots\, x_{Natom}, y_{Natom}, z_{Natom}\} \tag{8}$$

Under this basis set, $(\partial/\partial x_a, \partial/\partial y_a, \partial/\partial z_a)t$ describe the gradient of the transfer integral $t$ with respect to a selected atom $a$ displacement, and $\mathbf{R}_I$ is the atomic Cartesian displacements in dimer system of phonon modes $\{\mathbf{Q}_I^c\}$, i.e.

$$g^I = \nabla t \cdot \mathbf{Q}_I^c \tag{9}$$

The results of gradient are displayed in Figure 7 where the direction of the gradient is highlighted by red arrows.

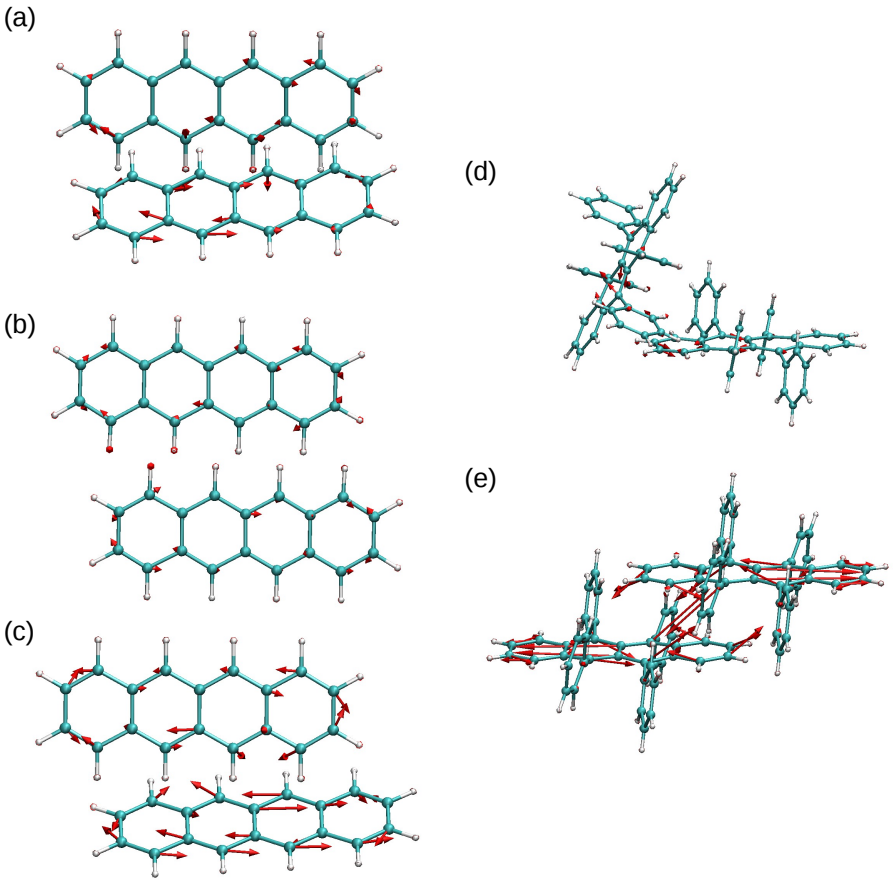


Figure 7: Gradient results (red arrows) for (a) tetracene dimer12, (b) tetracene dimer13, (c) tetracene dimer23, (d) rubrene dimer12 and (e) rubrene dimer13 based on $g^{i,0}$.

# References


(1) Aradi, B.; Hourahine, B.; Frauenheim, T. DFTB+, a Sparse Matrix-Based Implementation of the DFTB Method. *J. Phys. Chem. A* **2007**, *111*, 5678–5684.

(2) Frisch, M. J.; Trucks, G. W.; Schlegel, H. B.; Scuseria, G. E.; Robb, M. A.; Cheeseman, J. R.; Scalmani, G.; Barone, V.; Mennucci, B.; Petersson, G. A.; Nakatsuji, H.; Caricato, M.; Li, X.; Hratchian, H. P.; Izmaylov, A. F.; Bloino, J.; Zheng, G.; Sonnenberg, J. L.; Hada, M.; Ehara, M.; Toyota, K.; Fukuda, R.; Hasegawa, J.; Ishida, M.; Nakajima, T.; Honda, Y.; Kitao, O.; Nakai, H.; Vreven, T.; Montgomery, J. A., Jr.; Peralta, J. E.; Ogliaro, F.; Bearpark, M.; Heyd, J. J.; Brothers, E.; Kudin, K. N.; Staroverov, V. N.; Keith, T.; Kobayashi, R.; Normand, J.; Raghavachari, K.; Rendell, A.; Burant, J. C.; Iyengar, S. S.; Tomasi, J.; Cossi, M.; Rega, N.; Millam, J. M.; Klene, M.; Knox, J. E.; Cross, J. B.; Bakken, V.; Adamo, C.; Jaramillo, J.; Gomperts, R.; Stratmann, R. E.; Yazyev, O.; Austin, A. J.; Cammi, R.; Pomelli, C.; Ochterski, J. W.; Martin, R. L.; Morokuma, K.; Zakrzewski, V. G.; Voth, G. A.; Salvador, P.; Dannenberg, J. J.; Dapprich, S.; Daniels, A. D.; Farkas, Ö.; Foresman, J. B.; Ortiz, J. V.; Cioslowski, J.; Fox, D. J. Gaussian 09 Revision D.01. Gaussian Inc. Wallingford CT 2013.

(3) Abdulla, M.; Refson, K.; Friend, R. H.; Haynes, P. D. A first-principles study of the vibrational properties of crystalline tetracene under pressure. *J. Phys. Condens. Matter* **2015**, *27*, 3754021–37540210.

(4) Giannozzi, P.; Baroni, S.; Bonini, N.; Calandra, M.; Car, R.; Cavazzoni, C.; Ceresoli, D.; Chiarotti, G. L.; Cococcioni, M.; Dabo, I.; Dal Corso, A.; de Gironcoli, S.; Fabris, S.; Fratesi, G.; Gebauer, R.; Gerstmann, U.; Gougoussis, C.; Kokalj, A.; Lazzeri, M.; Martin-Samos, L.; Marzari, N.; Mauri, F.; Mazzarello, R.; Paolini, S.; Pasquarello, A.; Paulatto, L.; Sbraccia, C.; Scandolo, S.; Sclauzero, G.; Seitsonen, A. P.; Smogunov, A.; Umari, P.; Wentzcovitch, R. M. QUANTUM ESPRESSO: a modular and open-source

software project for quantum simulations of materials. *J. Phys. Condens. Matter* **2009**, *21*, 3955021–39550219.

(5) Lee, K.; Murray, E. D.; Kong, L.; Lundqvist, B. I.; Langreth, D. C. Higher-accuracy van der Waals density functional. *Phys. Rev. B* **2010**, *82*, 0811011–0811014.

(6) Baroni, S.; de Gironcoli, S.; Dal Corso, A.; Giannozzi, P. Phonons and related crystal properties from density-functional perturbation theory. *Rev. Mod. Phys.* **2001**, *73*, 515–562.